ELSEVIER

Design of Fiber-Reinforced DSP Mixes for Minimum Brittleness

D. Lange-Kornbak* and B.L. Karihaloo†
**Department of Civil Engineering, University of Sydney, Sydney, Australia; and †School of Engineering, University of Wales Cardiff, Cardiff, United Kingdom*

The limitations of the traditional material design approach in driving properties to extreme values and handling multiple design criteria and variables can be overcome by applying the optimization approach. Fiber-reinforced cement based composites based on strong aggregates and exhibiting approximately bilinear fiber pullout behavior are optimized in the present study for a given compressive strength f_c' with a view to maximizing their uniaxial tensile strength f_t' and fracture energy G_F. Relations for the bridging stresses prior to and during fiber pullout are established using fracture mechanics. The mix design leads to nonlinear, single, or multicriterion maximization problems for the objective functions f_t' and $l_{ch} = EG_F/f_t'^2$ (characteristic length), subject to an equality constraint on f_c'. In this way, optimal values for the microstructural parameters (fracture toughness of paste, length of fiber, and volume fractions and diameters of aggregate and fiber) are obtained. Advanced Cement Based Materials 1998, 7, 89–101. © *1998 Elsevier Science Ltd.*

KEY WORDS: Optimization, Micromechanics, Microstructural parameters, Fracture mechanics, Characteristic length, DSP, Fiber pullout, Tension softening

There is growing recognition in the structural design and research community of the fact that the implementation of a material/structural brittleness measure in the design of plain and reinforced concrete can improve structural reliability by providing uniform safety margins over a wide range of structural sizes and material compositions. The safety margin typically depends on the accuracy of the prediction of a structure's load-bearing capacity and on the assumptions made regarding the material properties, applicable analysis method, and the structural failure mode. Notwithstanding this knowledge, the current practice of design generally ignores the fact that the accuracy of assumptions and predictions is affected by the structural size and material composition. This assertion is supported by a substantial amount of experimental evidence (for a review, see reference [1]).

To describe the variations in the relative load-carrying capacity (i.e., the ratio of nominal strength to direct tensile strength) and the failure mode of concrete structures/specimens with the structural/specimen size and the material composition, principles of fracture mechanics have provided various brittleness measures (see reference [1] for a review). They consistently indicate that the characteristic length introduced in the fictitious crack model [2] is an appropriate measure for describing the effect of the material composition [1,3–5]. The characteristic length is given by:

$$l_{ch} = \frac{EG_F}{f_t'^2} \tag{1}$$

where E is the modulus of elasticity, G_F the specific fracture energy, and f_t' the direct tensile strength. As l_{ch} controls the nominal strength, failure mode, and crack growth (crack pattern), it ought to be taken into consideration in the design of concrete mixes. However, the traditional approach to design of concrete mixes drives only two mechanical properties, typically the compressive strength f_c' and the mix workability, to target values. This is due to the fact that this heuristic approach is unable to accommodate more than two design criteria. Recently though, Monteiro et al. [6] proposed a heuristic approach to design for target values of fracture mechanical properties through empirical relations (such as Abram's law, Lyse's law, and Molinari's law) based on the water/cement ratio w/c, cement content, and aggregate/cement ratio. However, by formulating the design problem as a mathematical optimization problem, efficient search techniques and convergence criteria can be brought to bear on the solution, so that problems involving many design variables and criteria can be successfully solved. The optimization approach to the design of cementitious materials has been reviewed by Brandt [7], and Brandt and Marks [8].

In the terminology of mathematical optimization, the mix variables (e.g., w/c, maximum aggregate size g,

Address correspondence to: Dr. B. Karihaloo, School of Engineering, University of Wales Cardiff, Queen's Buildings, P.O. Box 917, Cardiff CF2 1XH, United Kingdom.
Received June 2, 1997; Accepted September 29, 1997

ISSN 1065-7355/98/$19.00
PII S1065-7355(97)00057-6

volume fraction of fiber V_f, etc.) are called the design variables that control the mechanical response of the mix, such as E, G_F, f'_t, f'_c, and l_{ch}. The mechanical response parameters that are to be optimized (i.e., maximized, minimized, or driven to target values) are called the objective functions, which are expressed in terms of the design variables. It is often necessary to impose constraints in the form of upper and lower bounds on the design variables and/or the objectives. The solution of the optimization problem is usually obtained by nonlinear mathematical programming techniques that rely on Kuhn-Tucker optimality conditions and gradient search principles [9]. Several such techniques are available in a package developed by Vanderplaats [10].

The mathematical optimization techniques have not been widely used for the design of optimal cement based mixes. We mention here the few attempts that have been made in this direction. de Larrard and Sedran [11] attempted to maximize f'_c of a plain concrete mix by altering the amounts of aggregate, cement, microsilica, superplasticizer, and g. They first related these design variables to the maximum packing of particles and mix viscosity using heuristic arguments and experimental evidence. Voznesensky and Lyashenko [12] also applied heuristic optimization to the design of a homogeneous mix. They expressed the "homogeneity" of the mix via empirical relations between the maximum f'_c or minimum f'_c and their standard deviations and the amounts of stabilizer and superplasticizer. The first formal, as opposed to heuristic, mathematical optimization approach was taken by Marks and Potrzebowski (reported in Brandt [7]). They formulated a mathematical multicriterion optimization problem with f'_c and the cost of the mix as design criteria (objectives), which were related empirically to the design variables (e.g., volume fractions of sand, gravel, crushed stone, and cement). In another formal approach, Lange-Kornbak and Karihaloo [13] considered single and multicriterion optimization of f'_c, f'_t, and l_{ch} to obtain optimum combinations of w/c, g, and volume fraction of coarse aggregate V_c and fine aggregate V_s.

Hitherto, the optimization of fiber-reinforced cementitious composites has been concerned primarily with the maximization of G_F of the composite. Thus, Marks [14] attempted to minimize the strain energy of a model one-dimensional fiber system. Li et al. [15] solved what was essentially an optimization problem. They obtained approximate optimal values of fiber properties (e.g., aspect ratio) and frictional bond strength between fiber-matrix interface after first relating the objective function G_F to the fiber properties and imposing a constraint on the critical embedded length of the fiber. In a series of works, Brandt [7] addressed the problem of simultaneous optimization of G_F, f'_c, and first cracking strength

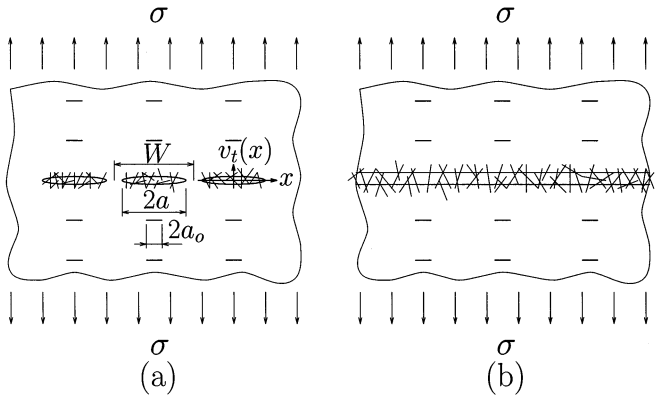

FIGURE 1. (a) Crack configuration prior to coalescence of cracks and (b) after coalescence of cracks during tension softening of fiber-reinforced quasi-brittle material.

of fiber-reinforced cementitious composites. These objective functions were related empirically to the various design variables, especially fiber parameters.

As shown in this work, the procedure recently developed by the authors for the establishment of the tension softening relation for fiber-reinforced cement-based mixes [16] has made it possible to design such mixes for minimum brittleness following the approach proposed by the authors for plain concrete mixes [13]. This will be demonstrated for fiber-reinforced mortars using cement, microsilica, and strong aggregates based on the DSP (Densified Systems containing homogeneously arranged ultra-fine Particles) concept [17].

Micromechanical Relations

In the following, we will first establish f'_t and G_F and then present relations for E and f'_c.

At initiation of localization in uniaxial tension, the effective stress in the localization zone equals the uniaxial tensile strength of the composite (Figure 1). The force transmitted by the localization zone is partly due to the unbroken matrix ligaments (P_b) and partly due to the fibers (P_f). Thus:

$$f'_t = \frac{P_b + P_f}{W^2} \tag{2}$$

where W is the center-to-center distance between the cracks. (Note that instead of W^2 in eq 2, Wt, where t is the thickness of the specimen, could have been used without altering the magnitude of the effective stress acting in the localization zone). If $f'_{t,b}$ is the uniaxial tensile strength of the matrix, and the length of the cracks at $\sigma = f'_t$ is independent of the volume fraction of fiber V_f, then $P_b = f'_{t,b}(1 - N_A A'_f)W^2$, where A'_f is the mathematical expectation of the area occupied by a

single fiber in the localization plane and N_A the number of fibers intersecting per unit of area of the localization plane. Note that in the determination of P_b it is not necessary to account for an increase in the size of the initial (intrinsic) cracks at the attainment of f_t' since in fiber-reinforced DSP composites the initial cracks do not propagate up to the attainment of f_t', but are supplemented by newly formed cracks [18]. This is the well-known multiple cracking behavior in the DSP matrix. For a three-dimensional, isotropic, uniform, and random fiber system $N_A = V_f/(2A_f)$ [19], with A_f the cross-sectional area of a single fiber. With $A_f' = 2A_f$, then:

$$\frac{P_b}{W^2} = f'_{t,b}(1 - V_f) \tag{3}$$

$f'_{t,b}$ follows from [13]:

$$f'_{t,b} = \frac{\eta K_{Ic,p}}{\sqrt{\pi r_o}}. \tag{4}$$

Here, $K_{Ic,p}$ is the fracture toughness of the cement-silica binder and η the toughening induced by the presence of fine aggregates, as only fiber-reinforced mortars are considered in this study. The half-length of cracks r_o is related to the maximum dimension of the aggregate R_{max} and the configuration of intrinsic microcracks caused by autogeneous deformation. Composites that do not suffer from such microcracks have $r_o = R_{max}/2$, whereas in the DSP composites studied here, $r_o = R_{max} + e/2$, with the edge-to-edge spacing between (spherical) aggregates $e = g_{av}(V_s^{-1/3} - 1)$; e follows from the definition of the volume fraction of aggregate as the volume of an aggregate particle of average size g_{av} relative to the volume of a representative composite spherical element with diameter $e + g_{av}$. R_{max} is somewhat larger than the nominal maximum aggregate size g; for $g \leq 4$ mm, a reasonable estimate is $R_{max} = 1.5g$. Because the DSP composites generally exhibit strong aggregate-matrix interfaces and contain small, strong aggregate particles (e.g., bauxite or korund), their toughness is enhanced by crack deflection, bridging, and trapping, such that [13]:

$$\eta = \sqrt{1.0 + 0.87V_s}\,\sqrt{\chi^2 + \frac{E_b'}{E_b}\frac{\pi {f'_{t,a}}^2 g_{av}(1 - \sqrt{V_s})(V_s - V_s^2)}{2(K_{Ic,p})^2}} \tag{5}$$

where

$$\chi = \left\{1 - \frac{(1 - V_s)\pi/4}{\ln\{[1 + \cos(\pi V_s/2)]/[\sin(\pi V_s/2)]\}}\right\}^{-1}$$

$$\frac{E_b'}{E_b} = 1 - \frac{\pi^2}{16}(1 - \nu^2)V_s$$

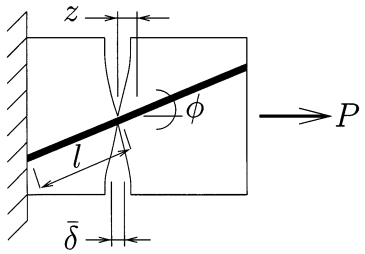

FIGURE 2. Single-fiber pullout with snubbing effect.

with E_b' the modulus of elasticity of the unreinforced composite with interfacial cracks and E_b that of the unreinforced composite without interfacial cracks. Poisson's ratio of the hardened paste is assumed equal to that of the mortar ν.

When a fiber is pulled out of a conventional cementitious matrix, a sudden drop in the pullout load is observed at the initiation of full slip. The type of DSP matrix studied here, however, exhibits a slow and gradual decrease in the pullout load [20]. A single fiber having a short embedment length l and bridging a crack with an effective opening $\bar{\delta}$ (Figure 2), therefore provides the bridging force:

$$P = \begin{cases} P_{max}\dfrac{\bar{\delta}}{\bar{\delta}_o}\,e^{f\Phi} & \text{for } \bar{\delta} \leq \bar{\delta}_o \\ P_{max}\dfrac{l - (\bar{\delta} - \bar{\delta}_o)}{l}\,e^{f\Phi} & \text{for } \bar{\delta} > \bar{\delta}_o \end{cases} \tag{6}$$

where $\bar{\delta}_o$ is the effective crack opening at the initiation of slip over l (assumed to occur at $\sigma = f_t'$) and $e^{f\Phi}$ accounts for the snubbing effect (fiber dowel action) arising when a fiber is not loaded in the direction of the initial straight fiber [21]; f is the snubbing friction coefficient. For an ideal brittle fiber-matrix interphase with toughness G_{ci}, the linear elastic fracture mechanics predicts that the maximum pullout load $P_{max} = \pi/2\sqrt{d^3 E_f G_{ci}}$, where d is the diameter and E_f the modulus of elasticity of the fiber [22,23]. However, due to slow crack growth, the resistance to propagation of the fiber-matrix interfacial crack (i.e., toughness) R_i increases as it propagates to the full length l, and G_{ci} should therefore be replaced by $R_i(l)$. Contrary to the conventional cementitious composites, the fiber-matrix interphase in DSP composites is not distinctly different from the matrix phase. Thus, $R_i(l) = (\eta'\eta K_{Ic,p})^2/E_b$, where $\eta' = \eta'(l)$ reflects the contribution of fibers to the toughening of the fiber-matrix interphase (primarily as a result of increased stiffness) and E_b is the modulus of elasticity of the matrix. This results in:

$$P_{max} = \frac{\pi}{2}\eta'\eta K_{Ic,p}\sqrt{d^3\frac{E_f}{E_b}}. \tag{7}$$

TABLE 1. Maximum pullout load P_{max} of a single fiber with embedment length l in an unreinforced DSP mix [20]

l (mm)	P_{max} (N)
6	23
12	31
18	45

It is expected that $\eta'(l)$ will be nearly independent of the type of aggregates present in the mix, so that it can be established, for instance, from the pullout tests performed by Al-Shannag [20] on single fibers with varying embedment length l in an unreinforced quartzite DSP mix having a volume fraction of fine aggregate $V_s = 0.508$, $g = 4$ mm, $E_b = 49100$ MPa, $E_f = 210000$ MPa, $d = 0.19$ mm, and $l = 6, 12, 18$ mm. The test results are reproduced in Table 1. The result for $l = 6$ mm is applicable to the present investigation, as it is restricted to fibers of length $L \leq 20$ mm, whereby the mathematical expectation of the embedded length $E(l) = L/4 \leq 5$ mm [16]. The assumption of a linear (l, P_{max}) relationship in the range $l \leq 6$ mm and the fact $P_{max} = 0$ kN at $l = 0$ mm suggest that:

$$\eta' = \alpha l \tag{8}$$

where α is an empirical constant to be determined. It will be determined for two cases. First, when η accounts for full crack trapping and second, when η disregards any crack trapping. The absence of crack trapping corresponds to $\chi = 1$ in the toughening ratio (eq 5). These two cases are studied because a crack propagating in the fiber-matrix interphase is likely to experience less trapping than that experienced by a crack propagating in the matrix phase. Thus, for $P_{max} = 23$ kN and $l = 6$ mm, eqs 7 and 8 give:

$$\alpha = \begin{cases} 342\text{m}^{-1} \text{ full crack trapping} \\ 932\text{m}^{-1} \text{ no crack trapping.} \end{cases} \tag{9}$$

In these calculations, it has been assumed that $K_{Ic,p} = 0.6$ MPa$\sqrt{\text{m}}$, the uniaxial tensile strength of the aggregate $f'_{t,a} = 10$ MPa, and the modulus of elasticity of the paste $E_p = 30000$ MPa. The tests by Al-Shannag [20] also indicate that P_{max}/l increases, if the fiber instead of being pulled out from a DSP matrix is pulled out from a fiber-reinforced DSP composite. This will cause α to increase further. The value $\alpha = 500\text{m}^{-1}$ has been assumed in the calculations to follow.

For frictionally or adhesively bonded fibers, the distribution of bridging stress along the crack (Figure 1a) is given by [16,21]:

$$p(\bar{\delta}) = \frac{2V_f}{LA_f} \int_{\phi=0}^{\pi/2} \int_{z=0}^{(L/2-\bar{\delta})\cos\phi} P(\bar{\delta}, \phi, z) \sin\phi \, dz \, d\phi \tag{10}$$

where z is the distance from the centroid of the fiber to the crack plane (see Figure 2). At the attainment of f'_t all fibers are subjected to $\bar{\delta} \leq \bar{\delta}_o$. Consequently, the distribution of bridging stress is (see Appendix):

$$p(\bar{\delta}) = \frac{h}{4} LV_f \alpha \eta K_{Ic,p} \sqrt{\frac{1}{d}\frac{E_f}{E_b}} \frac{\bar{\delta}}{\bar{\delta}_o} \tag{11}$$

where the snubbing factor $h = 2/(4 + f^2)(e^{f\pi/2} + 1)$. The effective bridging stress follows by regarding $\bar{\delta}$ as the effective deformation of the localization zone, namely [16]:

$$\bar{\delta} = \frac{f'_{t,b}}{E_b} L\left(1 - 2\,\frac{a}{W}\right) + \frac{2}{W}\int_{-a}^{a} v_t(f'_t, x)\,dx \tag{12}$$

with v_t the local half-opening of the crack such that:

$$\frac{P_f}{W^2} = p(\bar{\delta}). \tag{13}$$

The local half-opening of the crack v_t is determined by the numerical procedure outlined by Lange-Kornbak and Karihaloo [16]. Note that the maximum opening of the crack $\bar{\delta}_o = 2v_t^{\max}$. Equation 13 in combination with eq 3 yields the uniaxial tensile strength (eq 2) of the fiber composite.

For long fibers ($L \geq 3$ mm) and not too low a volume fraction of fiber ($V_f \geq 0.01$), the energy expended on the growth of discrete bridged cracks until the formation of a through bridged crack is an insignificant fraction (10%, at the most) of the total specific fracture energy G_F [16]. For a through crack with the inelastic crack opening $w = \bar{\delta} - \bar{\delta}_o$, the tension softening relation (cf. eq 39 in the Appendix):

$$\sigma(w) \approx 2hLV_f \alpha \eta K_{Ic,p} \sqrt{\frac{1}{d}\frac{E_f}{E_b}} \left\{\frac{1}{8} - \frac{1}{2L}\,w + \frac{1}{2L^2}\,w^2\right\} \tag{14}$$

results in

$$G_F = \int_{w=0}^{L/2} \sigma(w)\,dw \approx \frac{h}{24} L^2 V_f \alpha \eta K_{Ic,p} \sqrt{\frac{1}{d}\frac{E_f}{E_b}}. \tag{15}$$

Li [24] investigated the uniaxial compressive strength of fiber-reinforced composites by means of the well-

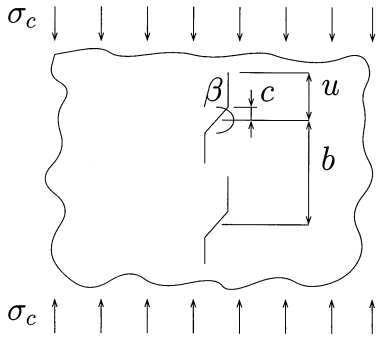

FIGURE 3. Wing crack model of Li [24] for fiber-reinforced concrete.

known wing crack model shown in Figure 3. The crack configuration (c, b, u) refers to lengths in the direction of applied compressive stress σ_c. u is the half-length of the individual cracks, b the crack spacing, and c the half-length of the inclined portion of the individual cracks. Li reported the stress intensity factor $K_I = \sqrt{2}c\tau/\sqrt{b\sin(\pi u/b)}$ and the shear stress acting on the inclined portion of the crack $\tau = 0.5\sigma(1-\mu) - \tau_B$, where μ is the coefficient of friction and τ_B the contribution to the shear stress from the fibers. The fracture toughness of the fiber composite K_{Ic} increases during crack growth, i.e., $K_{Ic} = K_{Ic}(u)$. The crack propagation criterion $K_I = K_{Ic}(u)$ yields:

$$\sigma_c = \frac{\dfrac{2}{\sqrt{2c}}\sqrt{b\sin\left(\dfrac{\pi u}{b}\right)}\,K_{Ic}(u) + 2\tau_B}{1-\mu}. \tag{16}$$

f_c' is now given by the peak stress of the $\sigma_c(u)$ curve. Li further identified τ_B as the stress provided by the fibers bridging the inclined portion of the wing crack and, with the aid of various approximations, a fiber bridging stress relationship was used to obtain an expression for τ_B. Moreover, K_{Ic} was assumed to depend linearly on u. Here, τ_B is the bridging stress $p(\bar{\delta})$ produced by the fibers when $\bar{\delta} > \bar{\delta}_o$, i.e., τ_B is given by (eq 14) assuming $w/L \approx 0$. It is noted that during the crack growth, $K_{Ic}(u)$ increases in accord with the well-known R curve behavior of cementitious composites. $K_{Ic}(u)$ will be estimated by solving the problem of Figure 1a as outlined by the authors [16]. This approximation is believed to be within an acceptable margin of error in view of the fact that the crack pattern observed under uniaxial tension is much the same as under uniaxial compression. This assertion appears to be justified by the experimental data presented in the next section. By letting the half-length of the wing cracks u increase incrementally by Δu, corresponding values of the compressive stress σ_c are calculated and the compressive strength is attained when the maximum value of σ_c is reached, i.e.:

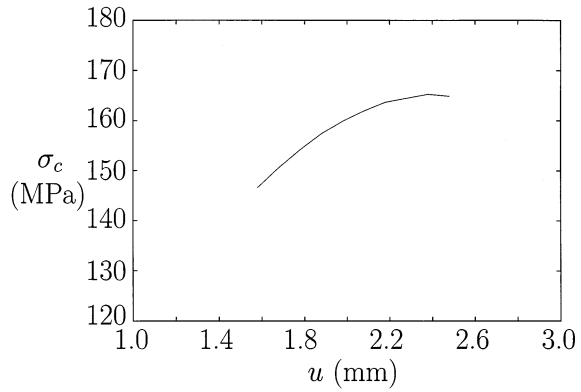

FIGURE 4. Applied uniaxial compressive stress vs. half-length of cracks. The uniaxial compressive strength is the peak value of the curve. In this example $V_s = 0.35$, $g = 1$ mm, $g_{av} = 0.375$ mm, $E_{agg} = 170$ GPa, $f_{t,a}' = 10.0$ MPa, $L = 6$ mm, $d = 0.15$ mm, $E_f = 210$ GPa, $V_f = 0.023$, $E_p = 30.0$ GPa, $K_{Ic,p} = 0.5$ MPa$\sqrt{\text{m}}$, $f = 0.9$, $W = 8.55$ mm, and $\mu = 0.5$.

$$f_c' = \max \sigma_c. \tag{17}$$

An example of the determination of f_c' is given in Figure 4. As the largest intrinsic cracks of size r_o (established above) are the ones that will eventually propagate, then $c = r_o\sqrt{2}/2$ and b is their center-to-center distance, i.e., the average center-to-center distance between the aggregates greater than g' and of average size g_{av}'. Therefore, $b = g_{av}' + e'$, where $e' = g_{av}'(V_s'^{-1/3} - 1)$, with $g_{av}' = g' + (R_{max} - g')/4$. The volume fraction of aggregates larger than g' for a Fuller grading is $V_s' = (1 - \sqrt{g'/R_{max}})V_s$ [25]. In the calculations to follow, it is assumed that $g'/R_{max} = 0.8$.

To simulate the multiple cracking in the fiber-reinforced DSP composite, the following relationship between the horizontal crack spacing W at the attainment of f_t' and the volume fraction of fiber has been established:

$$W = 2\,\frac{1.5g + e/2}{0.18 + 3.4V_f}. \tag{18}$$

This relationship has been found to provide good predictions. For instance, if the strain capacity $\epsilon_c = \epsilon|_{\sigma=f_t'} \approx \Delta H/H \approx w_t/H$, with H the vertical crack spacing (Figure 1a), then it is found that $\epsilon_c/(f_{t,b}'/E_b) = 1136.5\ \mu\text{strain}/(9.98\ \text{MPa}/55792\ \text{MPa}) = 6.4$, which agrees well with the findings of Tjiptobroto and Hansen [18] and Al-Shannag [20]. In the estimation of $\epsilon_c/(f_{t,b}'/E_b)$, the following mix and material parameters were used: $V_f = 0.12$, $K_{Ic,p} = 0.6$ MPa$\sqrt{\text{m}}$, $g = 4$ mm, $V_s = 0.35$, $E_{agg} = 170000$ MPa, $L = 6$ mm, $d = 0.15$ mm, $f = 0.9$, and $H = 1$ mm. Further evidence in support of the relationship (eq 18) is given below.

Fiber-reinforced and unreinforced mortar are regarded as two-phase systems with the modulus of elasticity given by [26,27]:

$$E = E_m \frac{n + \Theta + V\Theta(n-1)}{n + \Theta - V(n-1)} \tag{19}$$

where V is the volume fraction of the discrete phase (aggregates or fibers), Θ is a geometry function accounting for the configuration of the discrete phase, and n is the ratio of modulus of elasticity of the discrete phase to E_m, the modulus of elasticity of the continuous phase (cement-silica paste or mortar). For mortar ($E = E_b$), $E_m = E_p$, the modulus of elasticity of the paste, n is the ratio of modulus of elasticity of the aggregate particles E_{agg} to E_p, and:

$$\Theta = \frac{1}{2}[q + \sqrt{q^2 + 4n[1 - \eta_s(1 - V_s) - n\eta_s(V_s - 1)]}]. \tag{20}$$

Here, $q = \eta_s(1 - V_s) + n\eta_s(V_s - 1)$ and:

$$\eta_s = \frac{3A(1 + A)}{1 + A + 4A^2} \tag{21}$$

with A being the aspect ratio of the aggregate particles. For fiber-reinforced mortar, $E_m = E_b$, $n = E_f/E_b$, and the geometry function accounting for the configuration of fibers is:

$$\Theta = \frac{1}{2}\{\psi + n\psi' + \sqrt{(\psi + n\psi')^2 + 4n(1 - \psi - \psi')}\} \tag{22}$$

in which

$$\psi = \psi_o \frac{c_d - V_f}{c_d}$$

$$\psi' = \min\left(\psi_o \frac{V_f - c_D}{c_d}, 1\right)$$

$$\psi_o = \eta_f \tag{23}$$

$$c_d = \frac{\psi_o}{1 + \psi_o}$$

$$c_D = \frac{(2c_d)^{10}}{2}$$

and the aspect ratio $A = L/d$.

Verification of Micromechanical Relations

The accuracy of the above formulation is judged by comparing the model predictions with experimental data for fiber-reinforced DSP composites obtained by Knudsen et al. [28,29], Hansen [30], and Aarup [31]. The mix compositions used in their tests are denoted Mix I, Mix II, and Mix III, respectively. The values of the microstructural parameters of the mixes are given in Table 2. The values of E_{agg}, E_p, $K_{Ic,p}$, f, and μ have been assumed as follows. The modulus of elasticity of the DSP paste is assumed to be slightly higher than that measured on conventional cement-silica paste [32] and is $E_p = 30$ GPa throughout this study, irrespective of any variations in the composition of the paste. The modulus of elasticity of the aggregate $E_{agg} = 170$ MPa was estimated such that reasonable predictions of the overall modulus of elasticity E were obtained. For cement paste, $K_{Ic,p}$ increases with decreasing water/cement ratio [13]. For DSP paste, a similar trend is expected for a decreasing water/binder ratio, and the minimum value of $K_{Ic,p}$ is therefore taken to be 0.4 MPa$\sqrt{\text{m}}$, which corresponds to a conventional cement paste having w/c = 0.25. f has been chosen slightly higher than the value $f = 0.75$ for conventional fiber-matrix interfaces [33]. For conventional cementitious composites, the coefficient of friction μ of cracks has been reported to range from 0.4 to 0.6 and to increase with increasing g [34,35]. Accordingly, the relation $\mu = (1 + 0.2g)/3$ has been chosen, such that $\mu = 0.6$ (0.4) for $g = 4$ mm (1 mm). Finally, $g_{av} = (1.5/4.0)g$ is assumed.

The predicted properties of the matrix (i.e., the composite exclusive of the fibers) of the three mixes are presented in Table 3. Tables 4 and 5 provide a comparison of theoretical and experimental properties of the

TABLE 2. Microstructural parameters of Mix I [28,29], Mix II [30], and Mix III [31]

Microstructural Parameter	Mix I	Mix II	Mix III
V_s	0.40	0.35	0.39
g (mm)	4.0	1.0	4.0
g_{av} (mm)	1.5	0.375*	1.5*
E_{agg} (GPa)*	170.0	170.0	170.0
$f'_{t,a}$ (MPa)*	10.0	10.0	10.0
L (mm)	12	Variable	6
d (mm)	0.40	0.15	0.15
E_f (GPa)	210.0	210.0	210.0
V_f	0.02	Variable	0.12
E_p (GPa)*	30.0	30.0	30.0
$K_{Ic,p}$ (MPa$\sqrt{\text{m}}$)*	0.6	0.5	0.7
f*	0.9	0.9	0.9
μ*	0.6	0.4	0.6

*Indicates assumed value.

TABLE 3. Predicted properties of the matrix of Mixes I, II, and III

Mix	E_b (MPa)	$f'_{t,b}$ (MPa)	η
I	64363	8.61	2.014
II	59267	13.63	1.920
III	63321	9.94	1.997

fiber-reinforced composite. In converting to uniaxial tensile strength, the flexural tensile strength data obtained for Mix II are multiplied by the factor 0.695 chosen such that the experimental f'_t coincides with the theoretical value $f'_t = 13.6$ MPa for $V_f = 0$. Moreover, the compressive strength of Mix III (Table 4) measured on 45 × 90 mm cylinders is converted to that measured on 100 × 200 mm cylinders by dividing by the factor 1.2 [31]. Furthermore, $K_{Ic,p}$ of this mix is increased over that of Mix I, since it was tested at a more mature age.

Table 4 confirms good agreement between measured and predicted properties of Mix I and Mix III. As expected, the predicted uniaxial compressive strength is considerably lower than the measured compressive strength under almost-uniaxial compression [36]. The difference is particularly pronounced because DSP composites produce a high frictional restraint at the ends of the specimen.

Table 5 shows that the predictions for Mix II agree well with the measurements, except for the composition having (L, V_f) = (12.7 mm, 0.035). This may be due to processing difficulties. Exceptions are also the mixes with (L, V_f) = (6.0 mm, 0.046) and (12.7 mm, 0.023), since the uniaxial compressive strength determined theoretically is noticeably lower than the strength measured under almost-uniaxial compression as described above. The reason for this discrepancy is the short curing period of 30 days for these test specimens, as opposed to the 50 days (on average) for the remaining test specimens. The general underestimation of G_F is likely to be caused by $K_{Ic,p}$ actually being larger than for the other test specimens, due to a change in the curing conditions. If $K_{Ic,p}$ were increased from 0.5 to 0.7 MPa$\sqrt{\text{m}}$, the values of G_F would increase by a factor of 1.4 and yield the much improved predictions shown in the parentheses in Table 5 (the mix having (L, V_f) = (12.7 mm, 0.0122) again being an exception).

Apart from processing difficulties and different curing periods, the simplifications made in the model to simulate the complicated fracture behavior of fiber-reinforced concrete contribute to the discrepancies. For instance, the contribution from the matrix to the overall uniaxial tensile strength f'_t (eq 3) is based on the assumption that the length of cracks at $\sigma = f'_t$ is independent of the fiber volume fraction V_f. However, at relatively high V_f, the size of the cracks becomes comparable to the crack spacing, whereby $f'_{t,b}$ reduces below the value predicted by eq 4. Consequently, the contribution from the matrix to f'_t appears to be exaggerated. Tables 4 and 5 present data in support of this assertion.

TABLE 4. Predicted and measured properties of Mix I [28,29] and Mix III [31]

Mix	Property	Experimental	Theoretical
I	E (MPa)	65800	65841
	f'_t (MPa)	11.1	13.1
	f'_c (MPa)	204.8*	143.8
	G_F (N/mm)	13.67	13.92
III	f'_c (MPa)	310.7*	236.4

*Indicates almost-uniaxial compression.

Maximum Characteristic Length

In the above micromechanical relations, V_s is the ratio of the volume of aggregates to the volume of matrix (i.e., mortar) and V_f the ratio of the volume of fibers to the total volume of composite (i.e., mortar reinforced with fibers). These two design variables traditionally control the design of fiber-reinforced composites and they can be assumed to be either independent or dependent upon each other. In the former case, the fibers replace mortar such that V_s and the composition of the paste remain unaltered, as in the tests of Hansen [30]. In the latter case, the fibers replace aggregates, so that $\Delta V_s = -\Delta V_f$, as in the tests of Tjiptobroto and Hansen [18]. The present work, however, is a generalization of the former design approach in that all design variables V_f, V_s, $K_{Ic,p}$, g, L, and d are allowed to vary simultaneously (and independently) in order to achieve the most beneficial composition of the composite, i.e., the composition exhibiting the least brittleness.

The minimization of the material brittleness is approached by maximizing l_{ch} and f'_t (minimizing $-l_{ch}$ and $-f'_t$) simultaneously. This approach is used because of

TABLE 5. Measured [30] and predicted properties of Mix II

L (mm)	V_f	f'_t (MPa) Exp.	f'_t (MPa) Theo.	f'_c (MPa) Exp.*	f'_c (MPa) Theo.	G_F (N/mm) Exp.	G_F (N/mm) Theo.
3.0	0.065	15.5	18.0	170.2	155.1	5.84	3.82 (5.35)
	0.162	24.9	27.2	250.7	190.1	13.45	9.52 (13.33)
6.0	0.023	15.5	18.5	182.1	165.2	11.11	5.41 (7.57)
	0.046	29.3	23.5	173.1	181.3	19.33	10.82 (15.15)
	0.068	28.5	28.4	225.7	199.4	27.30	15.98 (22.37)
12.7	0.012	20.6	22.4	194.6	193.8	31.44	12.44 (17.42)
	0.023	26.3	29.2	176.1	226.9	35.91	24.21 (33.90)
	0.035	20.5	36.0	222.0	260.4	28.11	36.84 (51.58)

*Indicates almost-uniaxial compression.

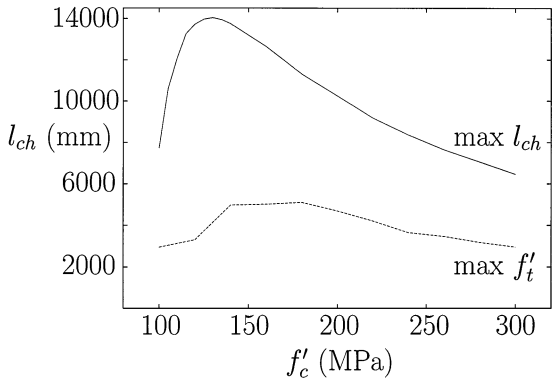

FIGURE 5. Characteristic length vs. compressive strength. The solid curve denoted "max l_{ch}" shows l_{ch} when it is maximized, and the dashed curve denoted "max f_t'" shows l_{ch} when f_t' is maximized.

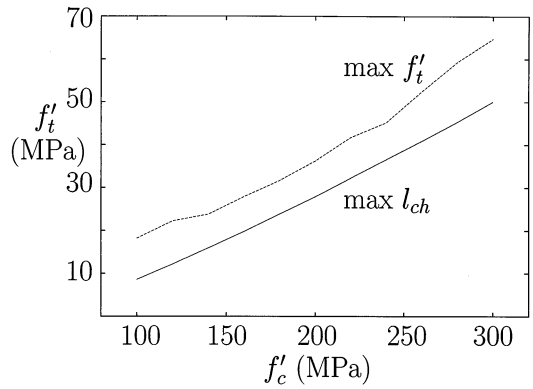

FIGURE 6. Direct tensile strength versus compressive strength. The dashed curve denoted "max f_t'" shows f_t' when it is maximized, and the solid curve denoted "max l_{ch}" shows f_t' when l_{ch} is maximized.

the competition between high material ductility l_{ch} and high strength f_t'. This can be illustrated by solving two single-criterion optimization problems. The first can be formulated as follows: For a prescribed f_c':

$$\text{Minimize} - l_{ch}(\mathbf{x}) \tag{24}$$

with

$$\{\mathbf{x}\} = \{V_s, g, L, d, V_f, K_{Ic,p}\}^T \tag{25}$$

by choosing the vector of design variables $\{\mathbf{x}\}$ in such a way as to meet the micromechanical relations [eqs 1–23], as well as prescribed lower and upper bounds on microstructural parameters (design variables):

$$\begin{aligned} 0.1 \leq\ & V_s \leq 0.7 \\ 1.5\text{ mm} \leq\ & g \leq 4.0\text{ mm} \\ 3.0\text{ mm} \leq\ & L \leq 20.0\text{ mm} \\ 0.1\text{ mm} \leq\ & d \leq 0.5\text{ mm} \\ 0.01 \leq\ & V_f \leq 0.16 \\ 0.4\text{ MPa}\sqrt{\text{m}} \leq\ & K_{Ic,p} \leq 1.0\text{ MPa}\sqrt{\text{m}}. \end{aligned} \tag{26}$$

T indicates transpose in eq 25. The second single-criterion optimization problem is equivalent to the above, except that $f_t'(\mathbf{x})$ is maximized. The solutions l_{ch} and f_t' of the above problems are given in Figures 5 and 6, respectively. Figure 5 shows that a high (maximum) f_t' will imply a small l_{ch}, whereas Figure 6 shows that a large (maximum) l_{ch} will imply a low f_t'. In view of this competition, a multiobjective optimization, in which both l_{ch} and f_t' are simultaneously maximized, is formulated.

The multiobjective optimization is solved by using standard methods available in the general purpose optimization package called the design optimization control program (DOC) [37], which is used together with the design optimization tools program (DOT) [38]. DOC solves the multiobjective optimization problem by using the so-called compromise programming technique. Here, a target (maximum) value for each of the objectives is required. Also, the worst known (minimum) value for each objective must be provided. Then DOC creates a composite objective:

$$F(\mathbf{x}) = \left\{ \sum_{j=1}^{2} \left[\frac{w_j(f_j(\mathbf{x}) - \max f_j)}{|\min f_j - \max f_j| + 0.001} \right]^2 \right\}^{1/2} \tag{27}$$

where $\{\mathbf{x}\}$ is the vector of design variables and w_j a weighting factor. In this investigation, f_t' and l_{ch} are considered to be of equal importance, i.e., $w_1 = w_2$. The double-criterion optimization problem can thus be formulated as follows: For a prescribed f_c':

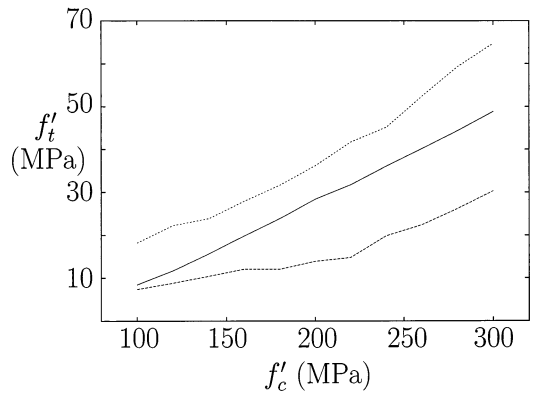

FIGURE 7. Relationship between direct tensile strength and compressive strength according to double-criterion optimization (solid). Also shown are the maximum (short dash) and minimum (long dash) direct tensile strengths needed in double-criterion optimization problem.

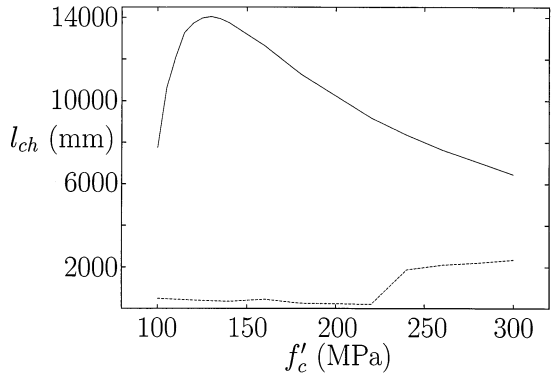

FIGURE 8. Optimum (solid), maximum (solid), and minimum (long dash) characteristic length vs. compressive strength according to double-criterion optimization. The optimum and maximum values are coincident.

$$\text{Minimize } F(\mathbf{x}) \tag{28}$$

with

$$\begin{aligned} \{\mathbf{x}\} &= \{V_s, g, L, d, V_f, K_{Ic,p}\}^T \\ f_1(\mathbf{x}) &= -l_{ch} \\ f_2(\mathbf{x}) &= -f'_t \\ w_1 &= w_2 = 1 \end{aligned} \tag{29}$$

by choosing the vector of design variables {**x**} in such a way as to meet the micromechanical relations [eqs 1–23], as well as the prescribed lower and upper bounds (eq 26) on microstructural parameters (design variables).

This nonlinear mathematical programming problem was solved by using the modified method of feasible directions because it was found to give optimal solutions with the least number of iterations, compared with the sequential linear and sequential quadratic programming techniques. As DOC requires an initial guess of values of the microstructural parameters in the vicinity of which an optimum is sought, these values were systematically varied in order to ensure global optimal (or at least very strong local optimal) solutions.

The extreme values of f'_t required in the composite objective (eq 27) are shown in Figure 7. It can be seen that the extreme values of f'_t increase with increasing f'_c. However, for a prescribed f'_c, f'_t can attain any value between the extremes so that it does not necessarily increase with increasing f'_c. The extreme values of l_{ch} required in the composite objective (eq 27) are shown in Figure 8. The maximum value of l_{ch} decreases with increasing f'_c, except when f'_c is low, i.e., $f'_c < 120$ MPa, which is generally infeasible for fiber-reinforced DSP composites. Hence, it may be concluded that the maximum l_{ch} generally decreases with increasing f'_c for fiber-reinforced DSP composites. It can be seen that the

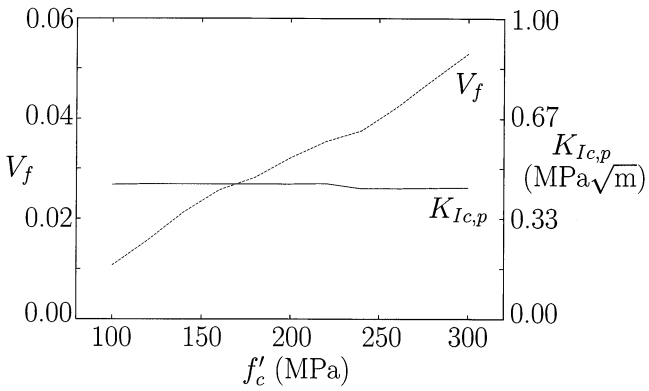

FIGURE 10. Optimum volume fraction of fiber and fracture toughness of paste vs. compressive strength.

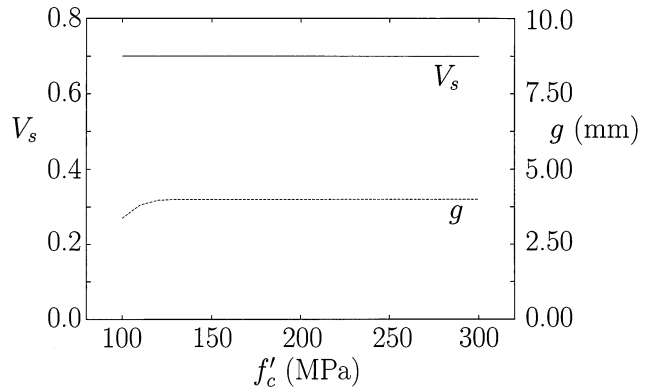

FIGURE 9. Optimum volume fraction of fine aggregate and fine aggregate size vs. compressive strength.

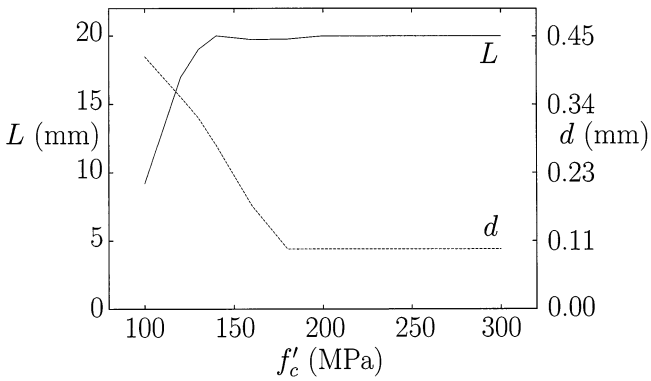

FIGURE 11. Optimum length and diameter of fiber vs. compressive strength.

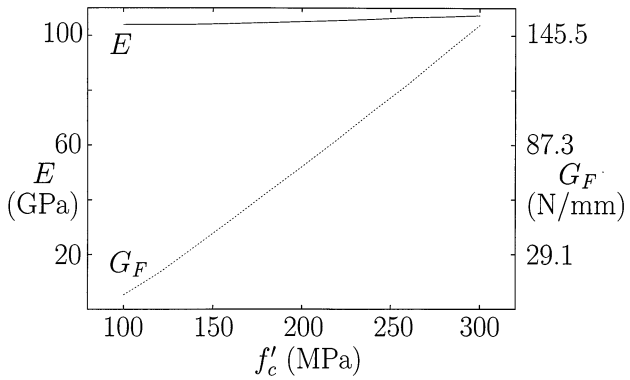

FIGURE 12. Optimum modulus of elasticity and fracture energy vs. compressive strength.

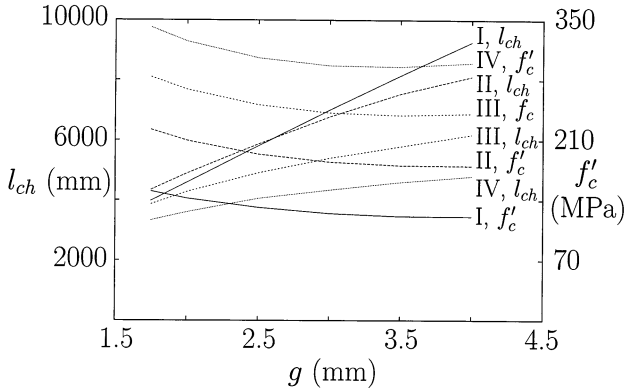

FIGURE 13. Sensitivity of optimum characteristic length and compressive strength to changes in maximum fine aggregate size for Mixes I, II, III, and IV of Table 6.

aggregate properties (Figure 9) and those of the paste represented by $K_{Ic,p}$ (Figure 10) essentially remain constant in the entire range of f_c' studied here; $V_s = 0.7$, $g = 4.0$ mm, and $K_{Ic,p} \approx 0.44$ MPa$\sqrt{\text{m}}$. Therefore, the most effective means of controlling the properties of the mix appears to be the variation of the fiber properties V_f and L/d, cf. Figures 10 and 11, respectively. To increase f_c', the fiber aspect ratio L/d will quickly increase towards its maximum value, while the volume fraction of fiber V_f will increase steadily. This results in significant increases in G_F, but negligible increases in E, as shown in Figure 12. However, it also involves a marked increase in f_t', so that l_{ch} will decrease with increasing f_c', as per Figures 7 and 8, respectively.

Finally, it should be emphasized that the optimum combination of microstructural parameters is the same in the double-criterion optimization problem of simultaneous maximization of l_{ch} and f_t', as in the single-criterion optimization problem of maximizing l_{ch}. This finding was also made for plain concrete mixes [13].

Sensitivity of Optimal Mixes

The effect of a change in the value of a microstructural parameter on the optimum design may be assessed by varying that parameter, while retaining all other microstructural parameters at their optimum values. For this purpose, the four optimum mixes given in Table 6 are considered.

As seen from Figure 13, a variation in g has little effect on f_c'. l_{ch}, on the other hand, exhibits a weak to strong dependence on g, as V_f is increased (Mix I has highest V_f). The effect of V_s on f_c' is insignificant, whereas it has some effect on l_{ch} (Figure 14). Figure 15 suggests that l_{ch} becomes more sensitive to changes in L, when V_f attains a high value. The reverse trend applies to f_c', according to the same figure. The sensitivity of f_c' and l_{ch} to changes in d is high for mixes with small d as indicated in Figure 16. The variation of f_c' with V_f in Figure 17 and with $K_{Ic,p}$ in Figure 18 is essentially linear, but quite substantial. The same figures show that V_f and $K_{Ic,p}$ also have a significant effect on l_{ch}, especially at low values of the microstructural parameters. Moreover, the figures indicate that moderate values of V_f and $K_{Ic,p}$ are preferable, owing to the competition between high strength f_t' and high material ductility l_{ch}.

Concluding Remarks

This study has established a numerical model for the direct tensile strength and an analytical model for the specific fracture energy of fiber-reinforced composites, based on the principles of fracture mechanics. This was accomplished by developing relationships for the

TABLE 6. Mixes selected for studying the sensitivity of optimum characteristic length and compressive strength to changes in V_s, g, L, d, V_f, and $K_{Ic,p}$

Mix	V_s	g (mm)	$K_{Ic,p}$ (MPa$\sqrt{\text{m}}$)	V_f	L (mm)	D (mm)	f_c' (MPa)	l_{ch} (mm)
I	0.462	3.98	0.448	0.0157	16.96	0.353	120.0	9220
II	0.463	4.00	0.449	0.0282	19.76	0.100	180.0	7526
III	0.478	4.00	0.433	0.0376	20.00	0.100	240.0	6125
IV	0.477	4.00	0.436	0.0530	20.00	0.100	300.0	4810

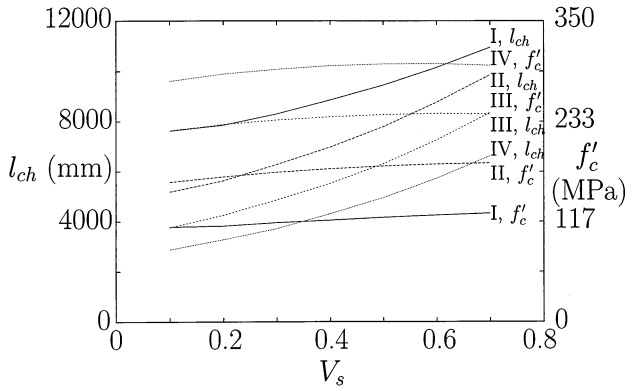

FIGURE 14. Sensitivity of optimum characteristic length and compressive strength to changes in volume fraction of fine aggregate for Mixes I, II, III, and IV of Table 6.

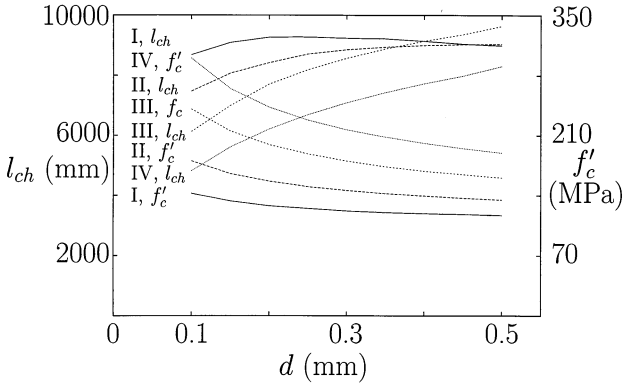

FIGURE 16. Sensitivity of optimum characteristic length and compressive strength to changes in fiber diameter for Mixes I, II, III, and IV of Table 6.

bridging stress provided by the fibers prior to, and during, unstable fiber-matrix interfacial cracking. The onset of unstable pullout of the fibers was assumed to occur at the attainment of the overall direct tensile strength of the composite. The empirical constant needed in the calculation of direct tensile strength and specific fracture energy was determined from test data for a DSP composite.

Furthermore, an existing model for the uniaxial compressive strength [24] was implemented by adapting an approximate, numerical method for the determination of the increase in the fracture toughness during the growth of wing cracks, as developed by the authors [16].

The models for direct tensile strength, uniaxial compressive strength, and the specific fracture energy were validated by available experimental data on fiber-reinforced DSP composites.

Finally, the models were used to design fiber-reinforced DSP composites for optimal macroscopic properties. It was found that mixes attain the same optimum combination of microstructural parameters when using either of the following two design criteria: (i) simultaneous maximization of the characteristic length and direct tensile strength for a prescribed compressive strength; and (ii) maximization of the characteristic length for a prescribed compressive strength. This conclusion was also reached for the optimization of plain concrete mixes in an earlier study by the authors [13]. Thus, the optimum (maximum) characteristic length of a fiber-reinforced DSP composite at any prescribed compressive strength is attained by mixes with a high content of the fine aggregates (V_s = 0.7), moderate toughness of the paste ($K_{Ic,p} \approx 0.44$ MPa$\sqrt{\text{m}}$), large size of the fine aggregates (g = 4 mm), and low-to-moderate content of fibers ($V_f \leq 0.055$). The most favorable way to attain the required compressive or direct tensile strength of a fiber-reinforced DSP composite is by varying the properties of the fibers. Thus, to gain

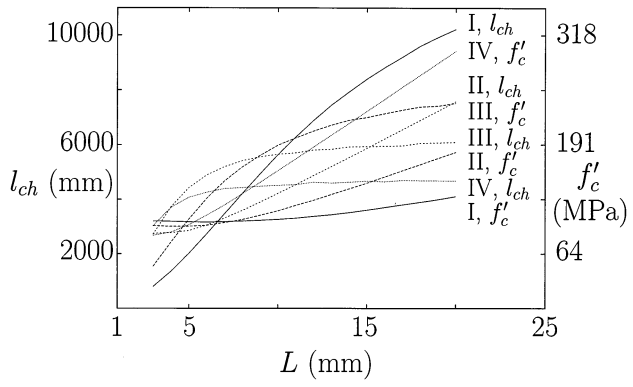

FIGURE 15. Sensitivity of optimum characteristic length and compressive strength to changes in fiber length for Mixes I, II, III, and IV of Table 6.

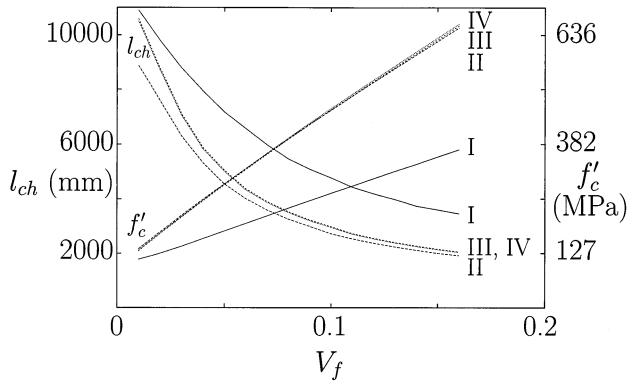

FIGURE 17. Sensitivity of optimum characteristic length and compressive strength to changes in volume fraction of fiber for Mixes I, II, III, and IV of Table 6.

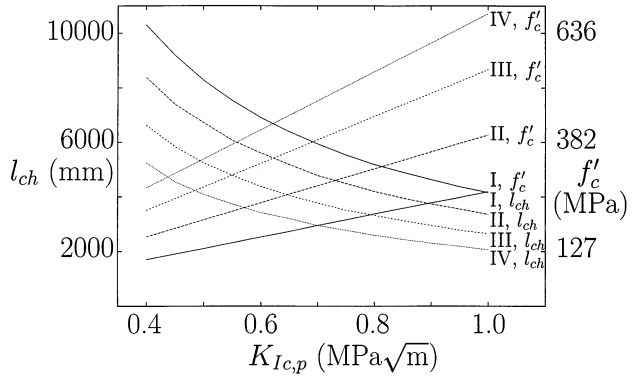

FIGURE 18. Sensitivity of optimum characteristic length and compressive strength to changes in paste toughness for Mixes I, II, III, and IV of Table 6.

additional strength, the fiber aspect ratio and the volume fraction of fiber must be increased.

Appendix

Bridging Stress Relationship Outside the Slip Zone ($\bar{\delta} \le \bar{\delta}_o$)

As $l = L/2 - z/\cos\phi$, eq 10 reads:

$$p(\bar{\delta}) = \frac{2V_f}{LA_f}\frac{\pi}{2}\alpha\eta K_{Ic,p}\sqrt{d^3\frac{E_f}{E_b}}\frac{\bar{\delta}}{\bar{\delta}_o}\int_{\phi=0}^{\pi/2}\int_{z=0}^{(L/2-\bar{\delta})\cos\phi} \times\left(\frac{L}{2}-\frac{z}{\cos\phi}\right)e^{f\phi}\sin\phi\,dz\,d\phi \tag{30}$$

where

$$\int_{z=0}^{(L/2-\bar{\delta})\cos\phi}\left(\frac{L}{2}-\frac{z}{\cos\phi}\right)e^{f\phi}\sin\phi\,dz = e^{f\phi} \times\sin\phi\left[\frac{L}{2}z-\frac{1}{2}\frac{1}{\cos\phi}z^2\right]_{z=0}^{(L/2-\bar{\delta})\cos\phi}$$

$$=\left(\frac{L^2}{8}-\frac{1}{2}\bar{\delta}^2\right)e^{f\phi}\sin\phi\cos\phi. \tag{31}$$

As $\sin\phi\cos\phi = \frac{1}{2}\sin\phi$, then:

$$\int_{\phi=0}^{\pi/2}\int_{z=0}^{(L/2-\bar{\delta})\cos\phi}\left(\frac{L}{2}-\frac{z}{\cos\phi}\right)e^{f\phi}\sin\phi\,dz\,d\phi = \left(\frac{L^2}{8}-\frac{1}{2}\bar{\delta}^2\right)\frac{1}{2}\int_{\phi=0}^{\pi/2}e^{f\phi}\sin 2\phi\,d\phi \tag{32}$$

with the snubbing factor h defined by:

$$\int_{\phi=0}^{\pi/2}e^{f\phi}\sin 2\phi\,d\phi = \frac{1}{2}\left(\frac{1}{2}L-\bar{\delta}\right)\left[\frac{e^{f\phi}(f\sin 2\phi - 2\cos 2\phi)}{4+f^2}\right]_{\phi=0}^{\pi/2}$$

$$=\frac{2}{4+f^2}(e^{f\pi/2}+1)$$

$$= h \tag{33}$$

such that the fiber bridging relationship:

$$p(\bar{\delta}) = \frac{2h}{L}V_f\alpha\eta K_{Ic,p}\sqrt{\frac{1}{d}\frac{E_f}{E_b}}\frac{\bar{\delta}}{\bar{\delta}_o}\left(\frac{L^2}{8}-\frac{1}{2}\bar{\delta}^2\right)$$

$$\approx \frac{h}{4}LV_f\alpha\eta K_{Ic,p}\sqrt{\frac{1}{d}\frac{E_f}{E_b}}\frac{\bar{\delta}}{\bar{\delta}_o}. \tag{34}$$

Bridging Stress Relationship Inside the Slip Zone ($\bar{\delta} > \bar{\delta}_o$)

Equation 10 now reads:

$$p(\bar{\delta}) = \frac{2V_f}{LA_f}\frac{\pi}{2}\alpha\eta K_{Ic,p}\sqrt{d^3\frac{E_f}{E_b}}\int_{\phi=0}^{\pi/2}\int_{z=0}^{(L/2-\bar{\delta})\cos\phi} \times\{l-(\bar{\delta}-\bar{\delta}_o)\}e^{f\phi}\sin\phi\,dz\,d\phi \tag{35}$$

where the use of eq 31 leads to

$$\int_{z=0}^{(L/2-\bar{\delta})\cos\phi}\{l-(\bar{\delta}-\bar{\delta}_o)\}e^{f\phi}\sin\phi\,dz = \int_{z=0}^{(L/2-\bar{\delta})\cos\phi}\left(\frac{L}{2}-\frac{z}{\cos\phi}\right)e^{f\phi}\sin\phi\,dz - (\bar{\delta}-\bar{\delta}_o)\int_{z=0}^{(L/2-\bar{\delta})\cos\phi}e^{f\phi}\sin\phi\,dz$$

$$=\left(\frac{L^2}{8}-\frac{1}{2}\bar{\delta}^2\right)e^{f\phi}\sin\phi\cos\phi - (\bar{\delta}-\bar{\delta}_o)e^{f\phi}\sin\phi[z]_{z=0}^{(L/2-\bar{\delta})\cos\phi}$$

$$= e^{f\phi}\sin\phi\cos\phi \times\left\{\frac{L^2}{8}+\frac{1}{2}\bar{\delta}^2-\frac{L}{2}(\bar{\delta}-\bar{\delta}_o)-\bar{\delta}_o\bar{\delta}\right\} \tag{36}$$

such that,

$$\int_{\phi=0}^{\pi/2}\int_{z=0}^{(L/2-\bar{\delta})\cos\phi}\{l-(\bar{\delta}-\bar{\delta}_o)\}e^{f\phi}\sin\phi\,dz\,d\phi$$
$$=\left\{\frac{L^2}{8}+\frac{1}{2}\bar{\delta}^2-\frac{L}{2}(\bar{\delta}-\bar{\delta}_o)-\bar{\delta}_o\bar{\delta}\right\}$$
$$\times\int_{\phi=0}^{\pi/2}e^{f\phi}\sin\phi\cos\phi\,d\phi$$
$$=\left\{\frac{L^2}{8}+\frac{1}{2}\bar{\delta}^2-\frac{L}{2}(\bar{\delta}-\bar{\delta}_o)-\bar{\delta}_o\bar{\delta}\right\}\frac{1}{2}h. \quad (37)$$

Finally, the fiber bridging relationship:

$$p(\bar{\delta})=2hLV_f\alpha\eta K_{Ic,p}\sqrt{\frac{1}{d}\frac{E_f}{E_b}}\left\{\frac{1}{8}+\frac{1}{2L^2}\bar{\delta}^2-\frac{1}{2L}(\bar{\delta}-\bar{\delta}_o)-\frac{1}{L^2}\bar{\delta}_o\bar{\delta}\right\} \quad (38)$$

or in terms of inelastic crack opening $w=\bar{\delta}-\bar{\delta}_o$:

$$p(w)=2hLV_f\alpha\eta K_{Ic,p}\sqrt{\frac{1}{d}\frac{E_f}{E_b}}\left\{\frac{1}{8}-\frac{1}{2L}w+\frac{1}{2L^2}w^2-\frac{\bar{\delta}_o^2}{2L^2}\right\}. \quad (39)$$

For a through crack, the tension softening relation is thus $\sigma(w)=p(w)$. It is noted that $\sigma(w)=0$ when $w\approx L/2$ as $\bar{\delta}_o^2/(2L^2)\approx 0$.

References

1. Lange-Kornbak, D. *Ph.D. Thesis*; University of Sydney: Sydney, 1997.
2. Hillerborg, A.; Modéer, M.; Petersson, P.-E. *Cem. Concr. Res.* **1976,** *6*, 773–782.
3. Jenq, Y.S.; Shah, S.P. *ASCE J. Eng. Mech.* **1985,** *111*, 1227–1241.
4. Brühwiler, E.; Broz, J.J.; Saouma, V.E. *J. Mater. Civil Eng.* **1991,** *3*, 235–251.
5. Karihaloo, B.L. In *Size-Scale Effects in the Failure Mechanisms of Materials and Structures*; Carpinteri, A.; Ed.; E & F N Spon: London, 1996; pp 325–339.
6. Monteiro, P.J.M.; Helene, P.R.L.; Kang, S.H. *Mater. Struct.* **1993,** *26*, 443–452.
7. Brandt, A.M. *Cement-Based Composites: Materials, Mechanical Properties and Performance*; E & F N Spon: London, 1995.
8. Brandt, A.M.; Marks, M. *Compos. Struct.* **1993,** *25*, 51–60.
9. Vanderplaats, G.N. *Numerical Optimization Techniques for Engineering Design*; McGraw-Hill: New York, 1984.
10. Vanderplaats, G.N. *ADS—A FORTRAN Program for Automated Design Synthesis (version 2.00)*; Engineering Design Optimization Inc.: Santa Barbara, CA, 1987.
11. de Larrard, F.; Sedran, T. *Cem. Concr. Res.* **1994,** *6*, 997–1009.
12. Voznesensky, V.V.; Lyashenko, T.V. In *Brittle Matrix Composites 4*; Brandt, A.M.; Li, V.C.; Marshall, I.H.; Eds.; Elsevier: London, 1994; pp 255–263.
13. Lange-Kornbak, D.; Karihaloo, B.L. *Adv. Cem. Based Mater.* **1996,** *3*, 124–132.
14. Marks, M. In *Brittle Matrix Composites 2*; Brandt, A.M.; Marshall, I.H.; Eds.; Elsevier: London, 1989; pp 54–64.
15. Li, V.C.; Wang, Y.; Backer, S. In *Mat. Res. Soc. Proc. Vol. 211*; Boston, 1991; p 63.
16. Lange-Kornbak, D.; Karihaloo, B.L. *Cem. Concr. Compos.* **1997** (in press).
17. Bache, H.H. *CBL Report No. 40*. Aalborg Portland: Denmark, 1981.
18. Tjiptobroto, P.; Hansen, W. *ACI Mater. J.* **1993,** *1*, 16–25.
19. Stroeven, P. In *Fiber Reinforced Cementitious Materials*; Mindess, S.; Skalny, J.; Eds.; Elsevier: London, 1991; pp 177–188.
20. Al-Shannag, M.J. *Ph.D. Thesis*; University of Michigan: Michigan, 1995.
21. Li, V.C.; Wang, Y.; Backer, S. *J. Mech. Phys. Solids* **1991,** *5*, 607–625.
22. Balaguru, P.N.; Shah, S.P. *Fiber-Reinforced Cement Composites*; McGraw-Hill: New York, 1992.
23. Karihaloo, B.L. *Fracture Mechanics and Structural Concrete*; Longman Higher Education: United Kingdom, 1995.
24. Li, V.C. *Cem. Concr. Compos.* **1992,** *14*, 131–141.
25. Mindess, S.; Young, J.F. *Concrete*; Prentice-Hall, Inc.: Englewood Cliffs: NJ, 1981.
26. Nielsen, L.F. *Tech. Rep. No. 208*; Build. Mat. Inst.: Tech. Un. Denmark, 1990 (in Danish).
27. Nielsen, L.F. *Tech. Rep. No. 264*; Build. Mat. Inst.: Tech. Un. Denmark, 1992.
28. Knudsen, M.; Sørensen, E.V.; Andersen, L. *Tech. Rep. Ducorit D4*; Densit A/S: Denmark, 1995.
29. Knudsen, M.; Andersen, L.; Sørensen, E.V. *Tech. Rep. Cylinder and Cube Compressive Strength of Ducorit D4 and S5*; Densit A/S: Denmark, 1995.
30. Hansen, A.S. *Tech. Rep. No. 132*; Build. Mat. Inst.: Tech. Un. Denmark, 1983 (in Danish).
31. Aarup, B. *Personal Communication*; Aalborg Portland A/S, Denmark, 1996.
32. Dela, B.F. *Tech. Rep. No. 333*; Build. Mat. Inst.: Tech. Un. Denmark, 1995 (in Danish).
33. Li, V.C.; Stang, H.; Krenchel, H. *Mater. Struct.* **1993,** *162*, 486–494.
34. Walraven, J.C. *ASCE J. Struct. Div.* **1981,** *ST11*, 2245–2270.
35. Divakar, M.P.; Fafitis, A. In *Micromechanics of Failure of Quasi-Brittle Materials*; Shah, S.P.; Swartz, S.E.; Barr, B.; Eds.; Elsevier Applied Science: London, 1990; pp 482–493.
36. Lange-Kornbak, D.; Karihaloo, B.L. *Report to RILEM Committee 148 SSC Strain Softening of Concrete*; University of Sydney: Sydney, 1994.
37. *DOC—Design Optimization Control*; Vanderplaats Research & Development Inc.: Colorado Springs, CA.
38. *DOT—Design Optimization Tools*; Vanderplaats Research & Development Inc.: Colorado Springs, CA.